The Pennsylvania State University
College of Earth and Mineral Sciences
Department of Materials Science and Engineering

Electrochemical Manipulation and Characterization of Organic Thiol Self-Assembled Monolayers on Metals and Semiconductors

A Thesis in Materials Science and Engineering

By Andrew C. Serino

Submitted in Partial Fulfillment of the Requirements for the Degree of Bachelor of Science in Materials Science and Engineering (Electronic & Photonic Materials Option)

Monday, December 13, 2010

I (we) approve this thesis: Date of Signature:

_____ _____

Paul S. Weiss, Professor
Thesis Advisor
Add other co-advisor signatures as needed

TABLE OF CONTENTS

ABSTRACT

Molecular self-assembly is a powerful technique for controlling and manipulating interfacial chemistry. Self-assembled monolayers are one-molecule thick molecular layers supported by substrates. Understanding the underlying features of the formation of such monolayers provides insight leading to the design of more complex assemblies. Assembly structures and function defined by the geometries of the molecular subunits, the interactions between the adsorbates and substrate, and intermolecular interactions between adsorbates. Electrochemical analysis can provide insight into each of these interactions and structures. Specifically, intermolecular hydrogen-bonding within **1ATC9** SAMs has dramatic effects on the properties, physical and electrochemical, of their assemblies. Rather than a simple one-electron reduction of the Au-S bond, **1ATC9** desorption is a two-step process, which can be interrupted. The first step converts the well-ordered monolayer into a distinctive striped assembly. Cyclic voltammetry was also used to reveal how dipole-dipole interactions between three adsorbed carboranethiol isomers altered their electrochemistry on Au{111}. Adsorbate-substrate interactions are a critically important feature to control and to understand as new substrate materials are used for self-assembly. Germanium is an exciting material for the extension of self-assembly. Due to the stronger bond between sulfur and Ge, **C12** desorbs at much higher potentials than it does on Au{111}.

ACKNOWLEDGMENTS

I acknowledge my mom, dad, and sister because without their unending support and direction this would have been impossible. I would also like to acknowledge my grandfather for the inspiration he provided me. I am sure my entire family will be proud of this.

I am incredibly fortunate for the opportunity Dr. Paul Weiss gave me to work in his group under the excellent guidance of Moonhee Kim and J. Nathan Hohman. I am very grateful to all of them for the time they spent as my mentors. I am deeply thankful for the help Moonhee provided me over the past two and a half years. I am very grateful for the training she provided me. I could always count on her to address my questions and to point me in the right direction. I could not have asked for a better teacher. I am very thankful for all of the help Nate has given me as well. He was also always there to provide me with guidance when I needed it or with an extra project to keep me thinking. I would also like to acknowledge everyone in the Weiss group who supplied me with support throughout this entire project. I thank Garrett Wadsworth, Jeffery Schwartz, Heidi Bednar, and Andrew Guttentag for their contributions to my research and Dr. Patrick Han for his help with revising this thesis. I am very grateful for the experience I have gained while working with all of them. I would like to thank Dr. Paul Weiss for supporting me through the summers of 2009 and 2010 at both Penn State and at UCLA.

I would like to acknowledge Penn State University and the department of Materials Science and Engineering and its faculty members for the incredible education that got me here. And of course, none of this would be possible without the support of the National Science Foundation and the California NanoSystems Institute.

LIST OF FIGURES

LIST OF TABLES

Chapter 1. Electrochemistry and Self-Assembly

1.1 Introduction into Electrochemistry

The fundamental process in electrochemistry is the transfer of electrons between the electrode surface (metal or semiconductor) and the molecules in a solution at the electrode surface. Electrochemistry can be used to obtain thermodynamic details of reactions by relating the potential change of a reaction to the free energy change, to generate an unstable intermediate, or to analyze a chemical system for trace amounts of metal ions or organic species.[1]

The standard electrode potentials (E°) are measured with respect to the standard hydrogen electrode (SHE), which undergoes the reaction:

$$2H^+_{(1.00\ M\ aq)} + 2e^- \leftrightharpoons H_{2\ (1\ atm)} \qquad (1)$$

This half-cell reaction is given an E° value of 0 V; every other electrochemical reaction is measured with respect to this standardization. Two independent half-cell reactions make up the overall chemical reaction. In most cases, the interest lies on only one of these half reactions and its corresponding electrode, the working electrode. In general, the standard working electrode is comprised of electrochemically stable materials (i.e., Pt, Au, Hg, and C). The other half-reaction occurs at the auxiliary electrode (or counter electrode). For example, hydrolysis under basic conditions involves two half-cell reactions:

$$2H_2O \leftrightharpoons 4e^- + 2OH^- + H_2 \qquad E^\circ = -0.83\ \text{V} \qquad (2)$$
$$OH^- + 4e^- \leftrightharpoons H_2O + O_2 \qquad E^\circ = -0.40\ \text{V} \qquad (3)$$

Reaction 2 occurs at the working electrode and Reaction 3 occurs at the auxiliary electrode. The purpose of the auxiliary electrode is to balance the redox reaction. An electrochemically inert material is used for this purpose as well. The third electrode, the reference electrode, is added to standardize the electrochemical measurements. This electrode is comprised of multiple, coexisting phases. For example Ag/AgCl electrode is a commonly used electrode, consisting of silver and silver chloride in a saturated aqueous solution of potassium chloride ($Ag/AgCl/KCl_{(sat)}$). This design allows the electrode to produce a well-known, fixed potential. This is desirable for an electrochemical experiment because any measured change in overall cell potential must then come from the working electrode; all measurements are made with respect to the reference electrode. The SHE is the internationally accepted reference electrode, but others are commonly used experimentally for their ease of use and stability, especially the saturated calomel electrode (SCE) or the Ag/AgCl electrode.[2]

1.2 Electrochemical System

A custom-built electrochemical cell is used with a BASi Epsilon potentiostat (Bioanalytical Systems Inc, West Lafayette, IN) (Figure 1.1). The area of the working electrode is ~0.5 cm^2, defined by a perfluoroelastomer O-ring from McMaster Carr (Cleveland, OH), mounted on top of the substrate inside the electrochemical cell, and electrochemically determined using the Randles-Sevcik equation. The electrochemical cell potential is applied to a modified working electrode and a Pt wire counter electrode, with a KCl saturated Ag/AgCl reference electrode. Electrochemical equipment is shown in Figure 1.2.

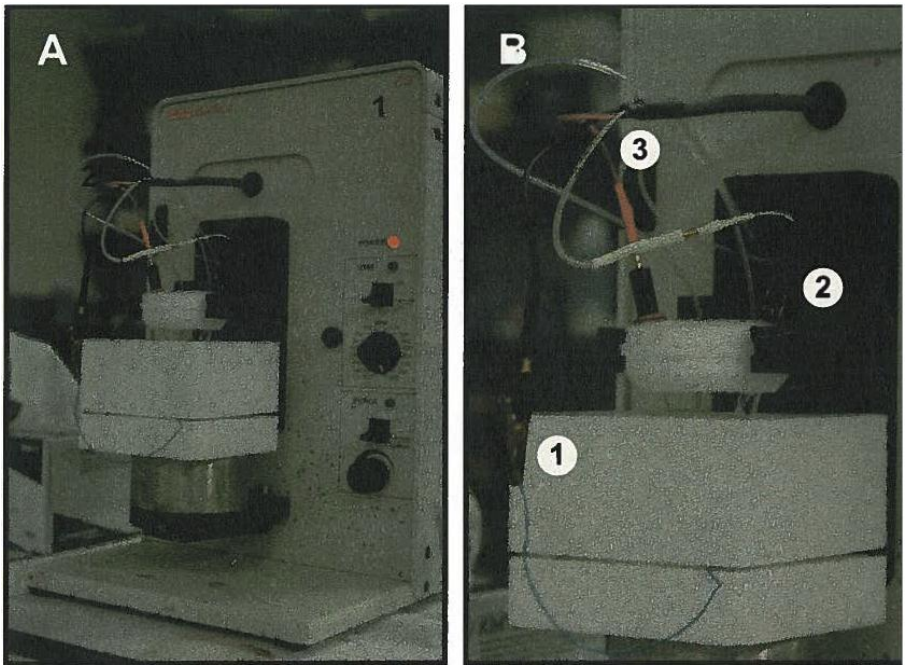

Figure 1.1. (A) BASi C3 cell stand and Teflon electrochemical cell. (B) Shows detailed view with connections to working (1), reference (2), and auxiliary (3) electrodes.

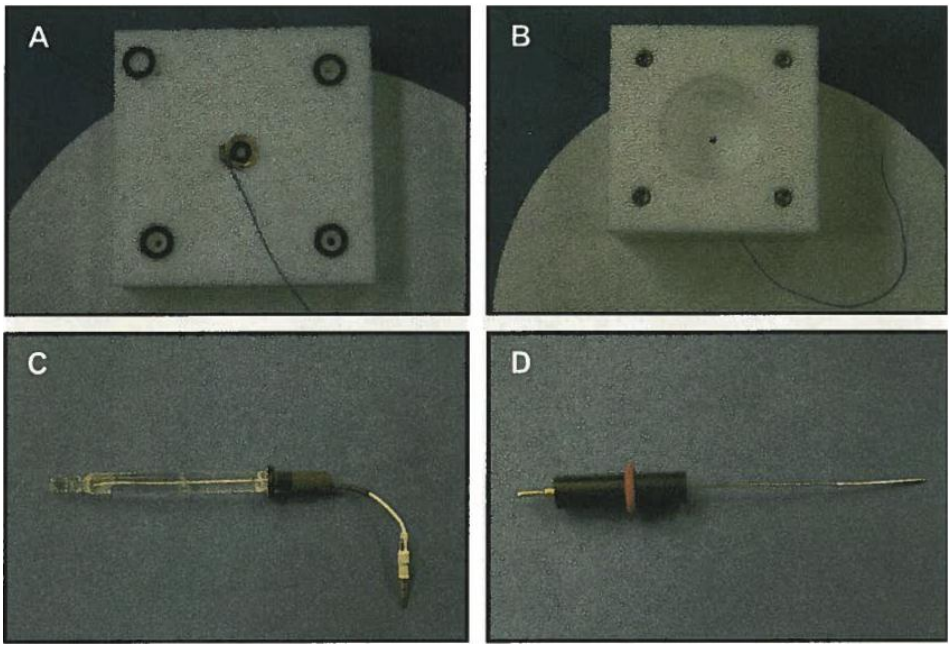

Figure 1.2. Teflon Electrochemical Cell (A and B) with working (A), reference (C), and counter (D) electrodes.

1.3 Self-Assembled Monolayers of Organic Thiols on Au

A self-assembled monolayer (SAM) is a single molecular layer that spontaneously assembles on metal substrates due to the balance between adsorbate-substrate attractions and intermolecular interactions. The SAM structure is dependent on the molecular shape of the adsorbate and the van der Waals interaction strength (see Figure 1.3 for *n*-alkanethiolate SAM assembled on Au{111}).[3,4] Thiol adsorbates form strong sulfur-gold bonds (~168 kJ/mol). The structure of the monolayer can be influenced by van der Waals forces, dipole-dipole interactions, and hydrogen bonding in the thiol backbone. These factors are affected by shape, length, functional group, and dipole moment in the adsorbate molecules. Changing any of these molecular characteristics alters the chemical, physical, and electrical properties of the material.

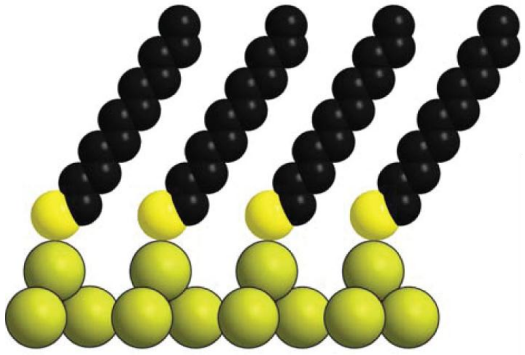

Figure 1.3. Schematic of *n*-alkanethiolate SAM structure on Au{111} showing well-ordered, close-packed structure as a result of van der Waals interactions between neighboring linear alkyl chains. Reproduced from reference 22, with permission.

The self-assembly of organic molecules offers a methodology to control interfacial wetting and adhesion,[3-5] nanoscale chemical patterning,[3-5] corrosion resistance,[6] sensitization for photon harvesting,[7] biocompatibility,[3-5,8] and molecular recognition for sensor applications.[8] Manipulating and controlling the SAM structure diversifies and simplifies the engineering strategy to construct low-cost and sustainably produced thin films. Thus, it is critical to design and to study molecules at the nano-scale, so that we can anticipate their interfacial behaviors to fabricate nanoscale electronics and other devices with better performance. For nano- or micro-electromechanical systems, these techniques can engender smaller devices using less material and resulting in smaller environmental impact. Self-assembled monolayers also offer a simple manufacturing process due to their spontaneous assembly. In essence, they construct themselves, and do not require external forces. Organic thiolate SAMs are also inexpensive[5] and versatile, with a large variety of available functional groups available for their exposed interface. Depending on the specific application and the final manufacturing process, the smaller amounts of raw materials combined with the self-assembly construction of the SAMs can contribute to a less expensive manufacturing process that requires less external energy to drive. The inherent efficiencies in this manufacturing process could lead to a smaller negative environmental impact and hence a more sustainable system.

1.3.1 Self-Assembly on Au{111}

The single crystal Au{111}surface is widely used as substrates for organic thiolate monolayers due to the ease of its preparation and the high-quality SAMs it supports. It is

relatively chemically and electrochemically inert making it useful for both self-assembly and electrochemistry. Further, these characteristics contribute to gold's biocompatibility.[3] While the adsorbate-substrate interaction is suitably strong to form stable monolayers, the complex formed between the gold and thiol is suitably mobile to allow diffusion during self-assembly to create well-ordered, stable structures. Due to this high affinity between gold and thiols and the diffusion of molecules on surfaces to improve order, a high-quality SAM can last for periods of days to weeks when in ambient conditions.[3]

1.3.2 *n*-Alkanethiols vs. Cage Thiols

In nature, self-assembly of molecules results in supramolecular structures.[9] Self-assembled monolayers offer an opportunity to understand the mechanisms and factors that affect self-assembly processes at large.[8-10] Tailoring the molecular structure influences the intermolecular interactions within monolayers; therefore, by changing the head group of the molecule or the substrate, the molecule–substrate interactions and molecular geometric factors alter the structural features of the film. Other factors, such as solvent and temperature, can also influence the interactions between molecules and the mechanism of assembly (or disassembly). Understanding the assembly process in SAMs can advance the use of these systems in several practical applications in nanoscale science, manufacturing, biology, and engineering.[3-5]

The simplest of the thiol based self-assembled monolayers are *n*-alkanethiols and are most commonly studied.[10-14] With a linear chain structure and *n* number of carbon atoms in the chain, it forms well-ordered, close-packed structures on Au{111} due to the interacting forces between the sulfur and gold and between alkyl chains. These high-quality monolayers of alkanethiols are straightforwardly prepared through solution and vapor depositions in ethanolic solutions for 12-24 hours.[3,10-14] Longer deposition times produce fewer defect sites. Alkanethiolates on Au{111} form a hexagonal $(\sqrt{3} \times \sqrt{3})R30°$ with respect to the underlying substrate. Molecules align themselves with 30° tilts from the normal to optimize intermolecular interactions.[15-17] Increasing the number of atoms in alkanethiols increases the van der Waals forces, and decreasing the number has the opposite effect.

Rigid, three-dimensional cage molecule SAMs provide a stark contrast to the linear n-alkanethiolates.[18-22] Adamantanethiol, a thiol derivative of a simple diamondoid, is one commonly used cage molecule (Figure 1.4). Changes in surface morphology are due to the bulky size of the cage molecule compared to the slender, linear chain of *n*-alkanethiol. The thiol position on the cage causes different tilt angles, which also changes the SAM surface structure. 1-Adamantanethiol (**1AD)** forms well-ordered, closely-packed structures without defects associated with molecular tilt. 2-adamantanethiol (**2AD**) adopts a tilted orientation on a Au{111} substrate. This minor molecular adjustment drastically changes the SAM surface morphology.

Figure 1.4. (A) 1-Adamantanethiol and (B) 2-adamantanethiol molecules.

Cage molecule surface coverage is lower than for *n*-alkanethiols (1.8 times fewer molecules per unit surface area) due to the larger size of the adamantane cage relative to the alkanethiols. The significantly higher intermolecular interactions in *n*-alkanethiols are due to larger contact areas between linear alkyl chains. Adamantanethiol has weaker interactions between neighboring molecules due to the low number of neighboring atoms. The weak interactions between adamantanethiolates have been exploited for chemical patterning techniques, specifically microdisplacement printing.[18,22] The adamantanethiolate monolayer is used as a protective layer, and is readily displaced by *n*-alkanethiols. It also provides lateral diffusion barriers for mobile ink molecules to create high-resolution patterns.

A second class of cage molecules is the carboranes (icosahedral dicarba-*closo*-dodecaboranes, $C_2B_{10}H_{12}$), composed of carbon, boron, and hydrogen. The positions of the carbon atoms can be altered, by design, by one or two boron atoms (Figure 1.5). Altering the position of these carbon atoms changes the dipole moment orientation and magnitude, thereby offering additional tunability in the form of electronic structure. Varying the electronic structure changes the molecule's dipole moment in orientation and intensity.[22-24]

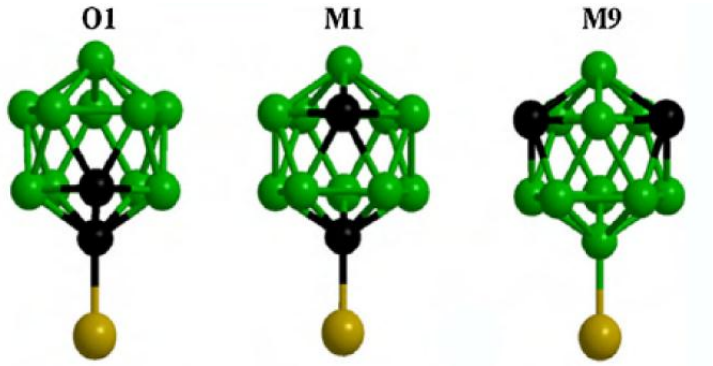

Figure 1.5: *o*-1-carboranethiol (**O1**) (a member of the *ortho*-carboanes with a thiol functionalization on the 1 position), *m*-1-carboranethiol (**M1**), and *m*-9-carboranethiol (**M9**) isomers shown here. Thiol positioning is noted numerically beginning with one of the carbon atoms.[22]

1.4 Electrochemistry of Organic Thiolate SAMs

A Au working electrode modified with a thiolated monolayer can be characterized electrochemically to determine the organization of molecules in a single-layer film, including surface coverage, molecular order, and the intermolecular interaction strengths.[11,25-28] Reductive desorption of thiolated species with applied cathodic potential is a one-electron reaction:

$$RS - Au + 1e^- \rightarrow RS^- + Au_0. \quad (4)$$

Electrolytic techniques are used to analyze thiolated working electrodes by applying voltage and monitoring current. Cyclic voltammetry (CV), a widely used electrolytic technique for studying thiolated SAMs,[10-13,28-34] applies a triangle potential waveform across the working and auxiliary electrodes and monitors the resulting current, shown in Figure 1.6. Peaks in current indicate chemical reactions (oxidation and reduction). Reduction of thiolated SAMs can be obtained using Equation 4.[35]

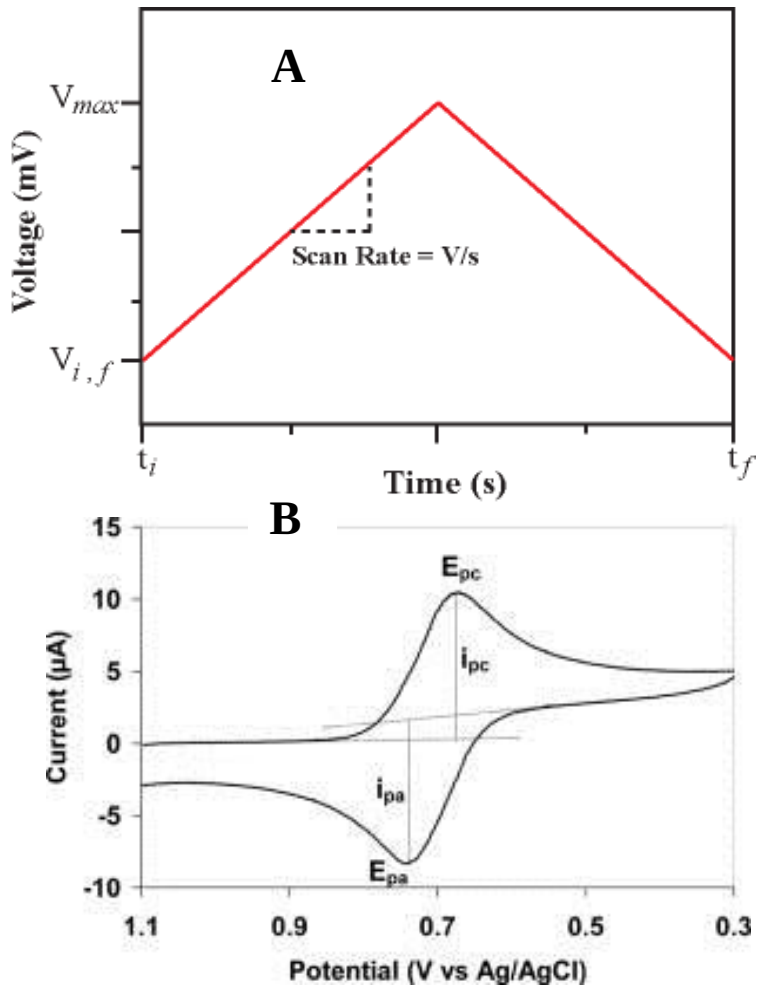

Figure 1.6. (A) The waveform of potential applied across the electrochemical cell over time, where the slope is the scan rate. Current is monitored as a function of potential to produce the generic cyclic voltammogram (B). Here, E_{pc} and i_{pc} are the cathodic peak potential and current, respectively and E_{pa} and i_{pa} are the anodic peak potential and current, respectively.

The peak potential gives insight into intermolecular interactions between similar molecules. The bonds between the gold and thiolated molecules are generally identical across varying molecular geometries, so the higher the potential needed to desorb the monolayer, the stronger the interactions between molecules in the SAM. Information about the ordering of the molecules on the substrate is provided by measuring the current full-width at half-maximum (fwhm). A narrow fwhm suggests a close-packed molecular structure. This is a result of molecules desorbing simultaneously due to increased intermolecular interactions from closer molecules.[11]

1.5 Thesis Overview

Understanding the adsorbate-substrate and intermolecular interactions within organic thiolates monolayers enable us to control and manipulate interfaces in electronic device applications. In this work, I have characterized the SAMs of three organic thiol molecules, namely, 3-mercapto-N-nonylpropionamide, *m-1*-carboranethiol, and *m-9*-carboranethiol, using electrochemical methods. Further, to study the effects of thiolate monolayers on a semiconducting germanium substrate, I have developed the methods for studying the electrochemistry of 1-dodecanethiolate films on Ge(111).

In order to benefit materials applications, self-assembly systems require a deeper fundamental understanding and further characterization. In conducting the experimental work discussed here, safety and environmental concerns were a large consideration. To uphold these environmental, safety, and ethical duties, preparations were made according to the Environmental Health and Safety at the Pennsylvania State University to ensure that the hazardous waste used in the following experiments is properly disposed of and that proper procedures were used in handling the material.

Chapter 2: Self-Assembled Monolayers of Amide-Containing Alkanethiols on Au{111}

2.1 Self-Assembled Monolayers of **1ATC9**

Self-assembled monolayers of amide-containing alkanethiolates are highly stable due to their inter-chain hydrogen-bonding interactions.[1] Previous studies[36-40] have shown that these molecules exhibit a slightly more complicated structure due to the interplay between the hydrogen-bonding network and van der Waals interactions in the hydrocarbon region. In this chapter, the electrochemical reduction of 3-mercapto-N-nonylpropioamide (**1ATC9**) in an alkaline aqueous solution will be discussed to differentiate between the hydrogen-bonding interactions within amide group and the inter-chain interactions that affect the structure and properties of the monolayer.

2.1.1 Self-Assembly of **1ATC9**

All **1ATC9** SAMs are prepared by submersing hydrogen-flame-annealed thin films of Au{111} on mica substrates (Agilent Technologies, Tempe, AZ) in a 1 mM ethanolic **1ATC9** solution. Clean substrates are placed in solution at room temperature or at 70 °C for 24 h. Following deposition, each sample is removed from solution, rinsed with ethanol (200 proof, Pharmaco, Brookfield, CT), and blown dry with nitrogen gas. The rinse/dry cycles are repeated three times. The samples are immediately used for scanning tunneling microscopic (STM) imaging and electrochemical measurements.

2.1.2 Hydrogen-Bonding Orientation in **1ATC9** Monolayers

The **1ATC9** prepared at room temperature (RT) has two domains. These domains differ in height by about ~1 Å, attributed to a difference in the molecular orientation and directionality of hydrogen bonding within the monolayer. The **1ATC9** sample prepared at the 70 °C shows only one phase in scanning tunneling microscopy (STM) images (Figure 2.1A). At this temperature the domain size increases and the number of defect sites decreases.[41,42]

It is postulated that at room temperature, the **1ATC9** molecules are trapped in either a less stable, upright and more protruding domain with *non-linear* hydrogen bonding (phase A) or in the more stable, tilted and less protruding domain (phase B) with **linear** hydrogen bonding.[40,43] At the higher temperature, 70 ºC the SAMs favor the more stable B phase to obtain more effective hydrogen-bonding interactions with linear orientation between amide groups.

2.2 Voltammetric Reductive Desorption

Cyclic voltammetry on **1ATC9** SAMs allow us to probe intermolecular interactions, specifically the hydrogen-bonding interations from the amide group. We expect the extra intermolecular interactions from the hydrogen-bonding networks in the amide group to increase molecular interaction strengths within the monolayers over those present in linear alkanethiol SAMs. However, cyclic voltammograms indicate that the amide group also increases the complexity of the system.

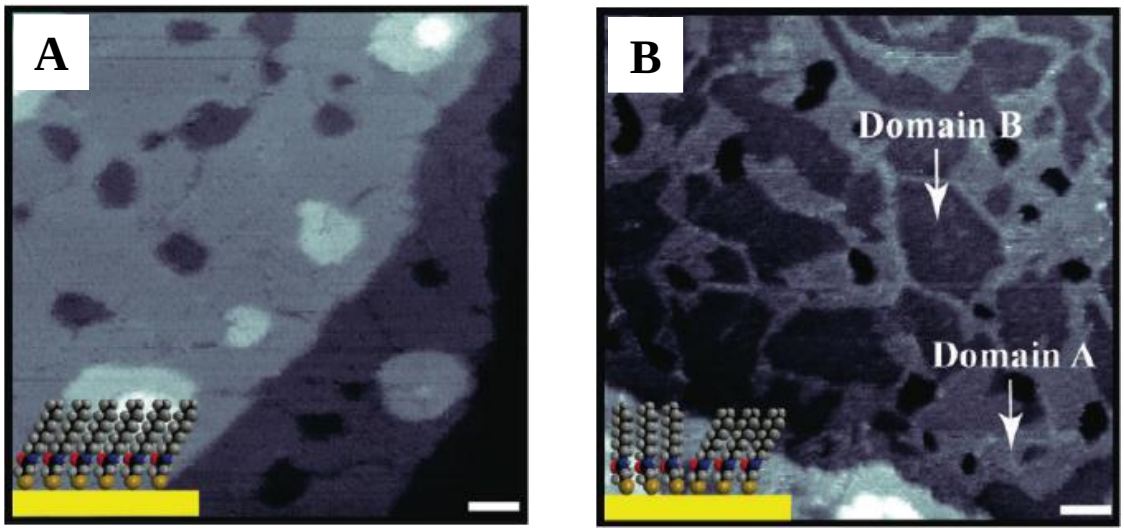

Figure 2.1. Scanning tunneling microscopy images of 3-mercapto-*N*-nonyl-propionamide (**1ATC9**) monolayers assembled at 70 °C (A) and RT (B). (All scale bars represent 100 Å). High temperature self-assembly (Figure 2.1A) provides enough diffusion energy to eliminate the non-linear hydrogen-bonding phase (domain A in Figure 2.1B), resulting in one phase. The spots in Figure 2.1A correspond to depressions (dark) and protrusions (light) in the gold surface. The insets in A and B show the different molecular orientations.[44]

2.2.1 Cyclic Voltammetry on **1ATC9** SAMs.

Using the equipment described in section 1.2, an electrochemical cell potential is applied with a Ag/AgCl saturated KCl reference electrode and a Pt wire counter electrode. The supporting electrolyte, an aqueous solution of 0.5 M KOH (99.99% Sigma-Aldrich, St Louis, MO), is prepared with deionized water (18.2M, Millipore Corp. Billerica, MA) and sparged with ultrahigh purity N_2 for 20 min. Cyclic voltammetry is performed at reductive potentials of -200 to -1300 mV with a scan rate of 20 mV/s. Baseline correction of voltammograms are done using GRAMS (Thermo Scientific, Location).[18,45] Seven representative cyclic voltammograms are selected to calculate the peak areas and standard deviations for the first peak at 70 °C, 20 for room temperature (RT). Nineteen representative cyclic voltammograms are selected for the second peak at 70 °C, and thirteen representative cyclic voltammograms at RT.

2.2.2 Reductive Desorption of **1ATC9** SAMs

Figure 2.2A shows representative cyclic voltammograms of single-component **1ATC9** on Au{111} deposited in solution at room temperature (blue trace) and at 70 °C (red trace) for 24 hours, analyzed in aqueous 0.5 M KOH solution. The voltammogram shows two reductive peaks, rather than the single peak observed in a one-electron desorption of short alkanethiolate SAMs depicted in Figure 2.2B.[35]

The presence of two peaks for RT and 70 °C **1ATC9** SAMs (Figure 9A) suggests that the number of phases and the number of cathodic peaks are unconnected. The presence of the double peak may originate from two different adsorption sites, or from differences in adsorption states.[11] As shown in Table 2.1, the first peak is centered on -920 mV and -943 mV for **1ATC9** SAMs formed at RT and 70 °C, respectively. Both SAMs assembled at 70 °C and RT show similar narrow fwhm and equivalent peak areas. This indicates that both monolayers are well-ordered and close-packed, so relative order is not responsible for the anomalous peak. The higher desorption potential for the 70 °C SAM area is a result of increased intermolecular interactions due to linear hydrogen bonding.

The second reductive peak is centered around -1100 mV for both SAMs likely originates from the desorption of all thiols left after the first reduction. This peak for both SAMs is substantially wider than the first reductive peak, indicating a decrease in packing order and density (Table 2.2). Peak areas also prove less-ordered **1ATC9** SAM structures after the first reduction, showing a substantial difference in desorbed thiols between **1ATC9** SAMs and **C12**.

Table 2.1: First reduction peak using cyclic voltammetry. Tables of tabulated values obtained.

Thiol Reduction	Average Peak Potential (mV)	Average Peak fwhm (mV)	Average Peak Current (μA)	Average Peak Area (μC)
3-mercapto-*N*-nonylpropionamide (**1ATC9**) 70 °C	-943 ± 6	39.7 ± 9.1	1.7 ± 0.5	3.4 ± 1.1
3-mercapto-*N*-nonylpropionamide (**1ATC9**) Room Temperature	-920 ± 6	39.3± 2.5	1.8 ± 0.3	3.4 ± 1.1

Table 2.2: Second reduction peak, corresponding to thiol desorption using cyclic voltammetry compared to **C12** reduction peak. Tables of tabulated values obtained.

Thiol Reduction	Average Peak Potential (mV)	Average Peak fwhm (mV)	Average Peak Current (μA)	Average Peak Area (μC)
3-mercapto-*N*-nonylpropionamide (**1ATC9**) 70 °C	-1111 ± 6	86.9 ± 25.9	1.5 ± 0.6	6.5 ± 3.4
3-mercapto-*N*-nonylpropionamide (**1ATC9**) Room Temperature	-1105 ± 5	106 ± 27	2.1 ± 0.6	11.0 ± 4.2
n-dodecanethiolate (**C12**)	-1098 ± 12	74 ± 11	5.3 ± 1.3	20.2 ± 4.9

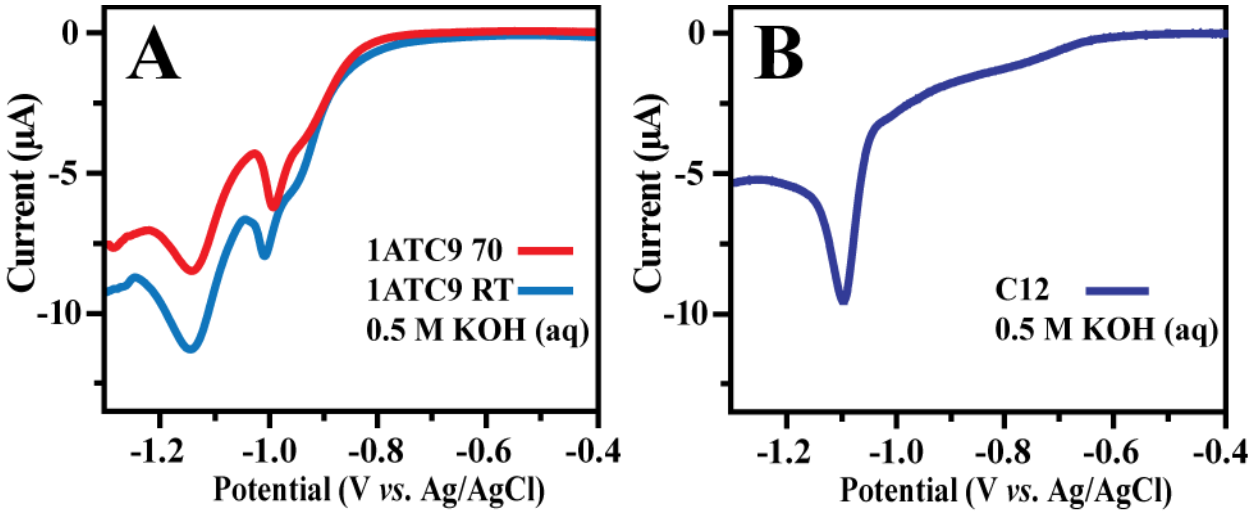

Figure 2.2. Cyclic voltammograms of **1ATC9** (70 ºC and RT) (A) and **C12** (B) SAMs on Au{111} with 0.5 M KOH aqueous solution.

2.3 Electrochemically Driven Surface Reconstruction

In order to understand the structural change after the first reductive desorption on **1ATC9** SAMs, we have conducted controlled potential electrolysis (CPE) on **1ATC9** SAMs. A CPE experiment involves the application of a constant potential, and the current response is measured as a function of time. A reductive potential of -960 mV is applied to **1ATC9** 70 °C SAMs for 120 s. To prevent KOH deposition, the samples are rinsed with a 50:50 deionized water/ethanol solution, followed by a rinse with ethanol, and finally blown dry with N_2. The SAMs were immediately imaged with the STM.

2.3.1 Controlled Potential Electrolysis on **1ATC9** SAMs

Figure 2.3 shows representative CPE graph of **1ATC9** SAMs. The figure shows an exponential decrease in current in response to an applied reductive potential of -960 mV. This correlates with a decrease in the reduction reaction rate.

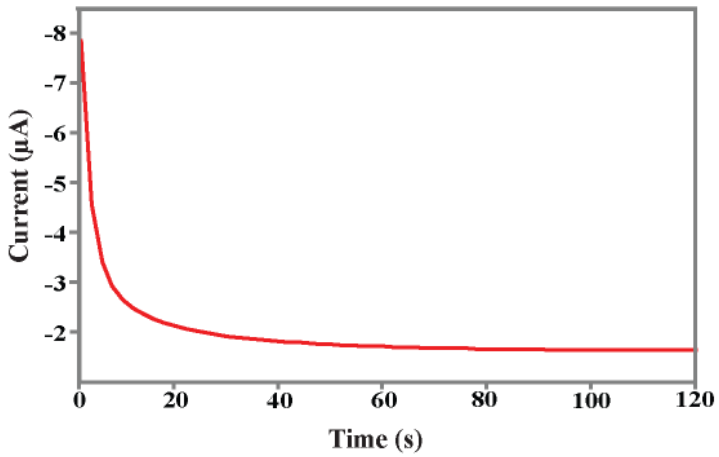

Figure 2.3. CPE graph of **1ATC9** SAMs. A reductive potential of -960 mV was applied for 120 seconds and the current response was measured.

2.3.2 Electrochemical Structural Manipulation on **1ATC9** Monolayers

Cyclic voltammetric results and Equation 4 suggest partial thiol desorption at an average of -943 ± 6 mV for 70 °C **1ATC9** SAMs (Table 2.1). This partial desorption creates vacancies, allowing the remaining molecules to reorganize. Controlled potential electrolysis is conducted at -960 mV for 120 s to drive the first reduction reaction, observed in the cyclic voltammograms in Figure 9A. The STM images in Figure 2.4 support this interpretation, showing the **1ATC9** monolayer structure is transformed into a stripped pattern. The protrusions indicate entire alkyl chains are physically bound to the Au surface, the lengths of which appear consistent with the average annealed **1ATC9** domain size (depicted in Figure 2.4 A). Depressions in between molecules on the SAM surface represent bare Au. The stripe patterns are oriented in three directions rotated by 120º with respect to each other. This reflects the 3-fold symmetry of the Au{111} surface. The high-resolution STM image in Figure 2.4 B shows the presence of the remaining, structurally reorganized **1ATC9** molecules and the bare gold surface.

Due to the presence of multiple reductive desorption peaks (Figure 9) of **1ATC9** SAMs, applying slightly higher voltage of the first desorption partially desorbs some weakly bound **1ATC9** molecules. The first reductive reaction changes the entire monolayer structures to compensate for the loss of molecules in the SAM. This controlled electrolysis on amide-containing alkanethiolate SAMs provides a straightforward means to fabricate nanoscale patterns on metal surfaces. In comparison to linear alkanethiolate SAMs, the second pseudo stable nanoscale structure is only possible in this **1ATC9** molecule, or at least amide-containing organic thiols that can form strong hydrogen-bonding interactions. This strong hydrogen bonding-network enables molecules to transform the structure spontaneously while maintaining hydrogen bonding interactions.

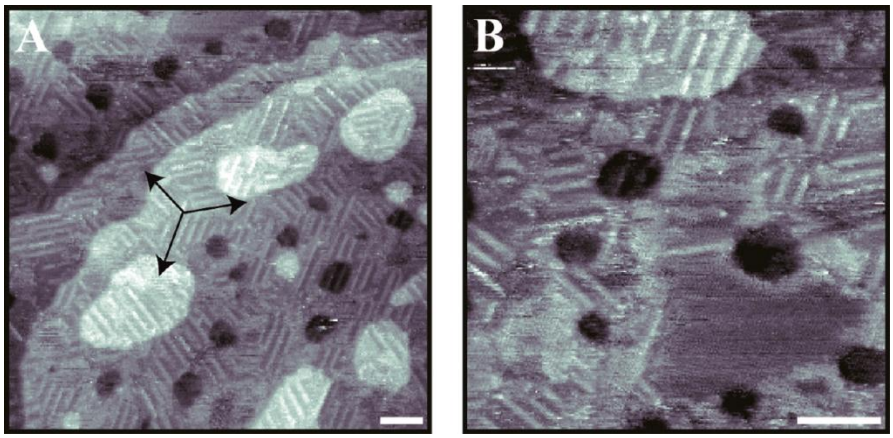

Figure 2.4**.** Scanning tunneling microscopy images of electrochemically processed **1ATC9** SAMs on Au{111}. (A) 1000 Å × 1000 Å, (B) 500 Å × 500 Å, sample bias -1.0 V, tunneling current 1.0 pA. All scale bars represent 100 Å. Prior to CPE, the **1ATC9** SAM has a single phase structure similar to that in Figure 2.1. The round protruding features correspond to Au adatom islands formed during self-assembly. Darkened indentations indicate spacing in between **1ATC9** molecules. As shown in Figure 2.4A, the striped patterns are oriented in three directions rotated by 120° with respect to each other.[44]

Chapter 3. Electrochemistry of Carboranethiol Self-Assembled Monolayers

3.1 Self-Assembled Monolayers of Carboranethiol on Au{111}

Carboranes are boron hydrogen cluster compounds where one or more boron atoms are replaced with a carbon atom. These result in thermally stable, rigid, and nearly icosahedreal (12-membered cage) compound. Thiol-functionalized carboranes make excellent molecular candidates for studying and extricating the effects of geometry and intermolecular interactions on self-assembly.[22,24] The icosahedral carborane has three positional isomers, *ortho*, *meta*, and *para*, depending on the relative position of the carbon atoms (Figure 3.1).

The different isomers of *meta* (**M1** and **M9**) and *ortho* (**O1**) carboranethiols have different dipole magnitudes and orientations. These dipole moments impact how the isomers assemble on the Au{111} substrate and the stability of the adsorbed monolayer. These differences can be observed electrochemically.

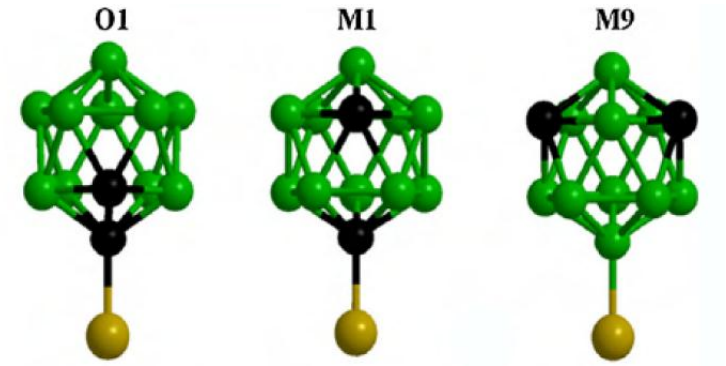

Figure 3.1: Schematic representation of carboranethiol isomers. From left to right, *o*-1-carboranethiol (**O1**) *m*-1-carboranethiol (**M1**), and *m*-9-carboranethiol (**M9**) isomers. The letter assignment denotes relative locations of the carbon atoms, and the numerical assignment corresponds to the position of the thiol relative to the carbon .[22]

Dipole moments in carboranes are typically oriented with the positive charge centered at the carbon atoms, with substituent's affecting the direction and magnitude. The **O1**, **M1,** and **M9** carboranethiol isomers (Figure 3.2) have dipole moments of 3.56,[46] 1.06, and 4.08 Debye,[22] respectively. STM images reveal that **M1** and **M9** (Figure 3.3) form loosely packed structures due to relatively weak intermolecular interactions between the carborane cages. The nearly identical geometries of the molecules show no apparent difference in surface morphology between a single component **M1, M9** SAMs or a dual component **M1**/**M9** SAMs. This indicates that molecular geometry is the dominant factor of the SAM structure, over dipole-dipole interactions. Since the molecular orientation is locked, we can presume that the dipole orientation will likewise be fixed, with **M1** dipoles aligned laterally, and **M9** dipoles aligned vertically (Figure 3.1). Similar to the *meta* isomers, we expect a similar surface structure in **O1** monolayers due to the nearly identical geometry. The dipole-dipole interactions of these carborane cages on Au{111} surface are characterized by cyclic voltammetry, complementing the previous STM and infrared analyses. The molecular structure of **O1** is similar to that of **M1**;

thus, we predict that its molecular dipole is laterally oriented to some degree. In this chapter, I attempt to analyze the effects of cage geometry within SAMs qualitatively and quantitatively and dipole interactions on their self-assembly using electrochemistry.

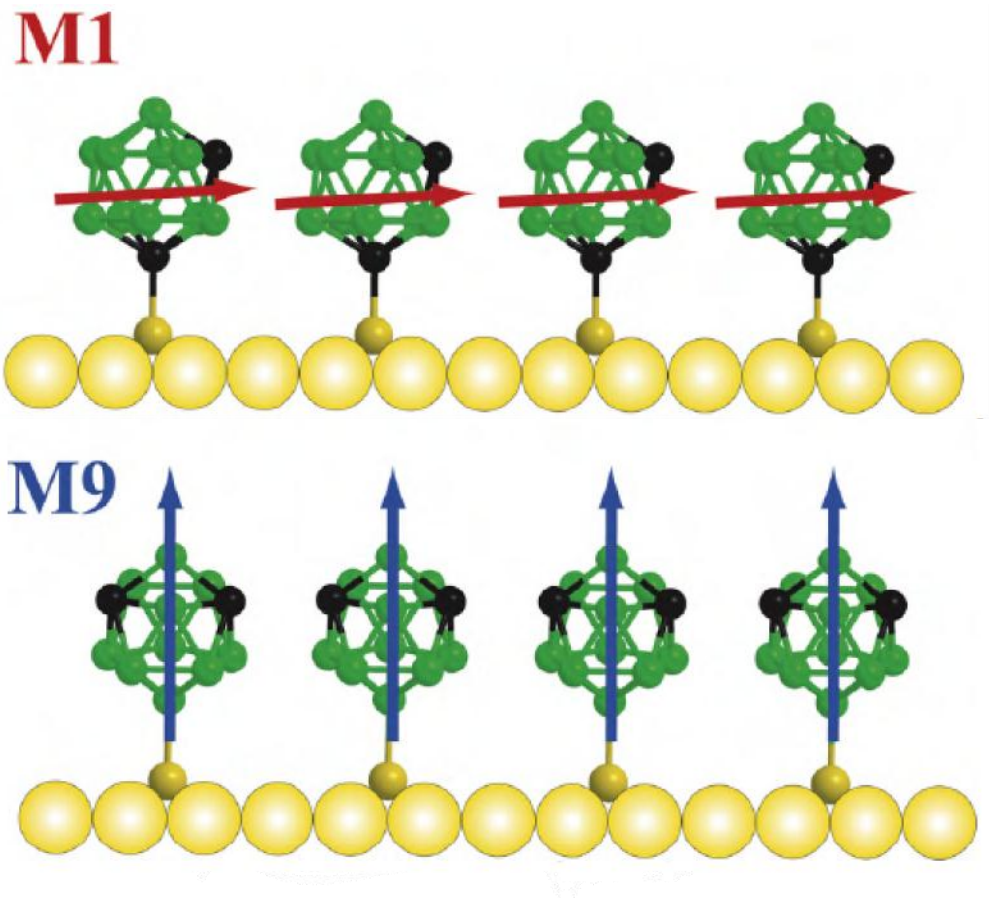

Figure 3.2: (Top) Schematic of **M1** assembled on Au{111}. Dipole moments align horizontally along the substrate. (Bottom) Schematic of **M9** assembled on Au{111}. Dipole moments align normal to the substrate.

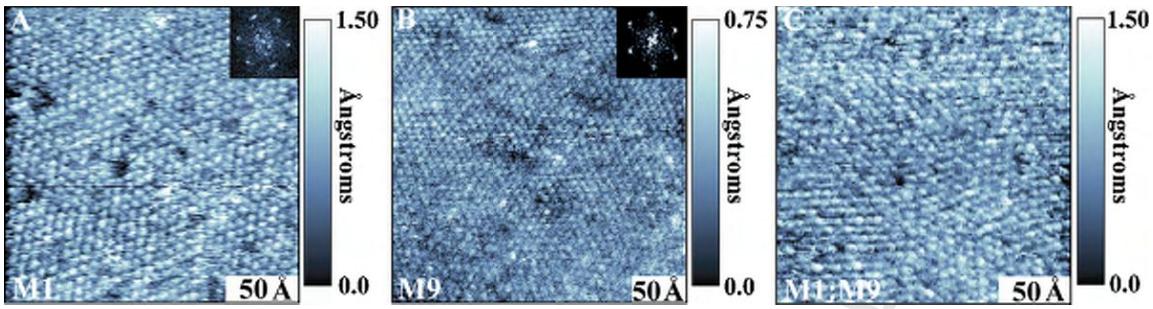

Figure (3.3): (A) STM images of **M1**, (B) **M9**, and (C) codeposited **M1** and **M9** SAMs on Au{111}. All three images show hexagonal molecular packing with identical lattices.[22]

3.2 Self-Assembly of Carboranethiols

Flame-annealed Au{111} on mica substrates were immersed in 1 mM ethanolic solutions of **M1**, **M9**, or **O1** carboranethiols at room temperature for 24 h. Assembly times longer than 24 hours gives higher ordering and stable SAMs.[22] Each sample was rinsed with ethanol as described earlier The samples were immediately used for electrochemical measurements.

3.2.1 Cyclic Voltammetry on Carboranethiolate SAMs

Cyclic voltammetry on **M1**, **M9,** and **O1** SAMs have been conducted as has been described in Chapter 1.2. Figure 3.3 shows the representative cyclic voltammograms of three carboranethiolate SAMs. The cathodic peak potential, areas, and fwhm with their respective standard deviations for **M1**, **M9**, and **O1** SAMs were calculated from an average of eight voltammograms and are given in Tables 3.1 and 3.2.

As shown in Figure 3.3, peak 1 is different for the three carboranethiol isomers. Peak 1 for **M1** is centered at -574 ± 26 mV, **M9** is centered at -635 ± 75 mV, and **O1** is centered at -501 ± 26 mV. An additional peak, peak 2, is seen in **O1,** not in the other two isomers, and is centered at -860 ± 3 mV. The cause for these cathodic currents is uncertain and requires further investigation.

Peak 3 is centered at -1079 ± 23 mV for **M1**, -1059 ± 23 mV for **M9**, and -1056 ± 5 mV for **O1** (Figure 3.4 and table 3.2). The cathodic reduction potential required to desorb **M1** is on average 20 mV stronger than required for **M9**. This can be attributed to **M1**'s laterally oriented, favorable head-to-tail dipolar interactions and **M9**'s unfavorable vertically oriented head-to-head dipole interactions (Figure 3.1). The reductive potential for **M1** and **M9** are significantly smaller than the values determined for **C12** (-1098 ± 12 mV), which is most likely a product of decreased packing density relative to the well-packed linear alkyl chains resulting in smaller van der Waals forces.

Alone, the small average desorption potential of **O1 (**-1056 ± 5 mV) indicates that the dipole orientation and magnitude has given weaker intermolecular interactions than **M1** and **M9** when assembled. The dipole moment of **O1** is either oriented vertically or the magnitude is negligible. This determination is complicated by the as yet unexplained appearance of peak 2 in **O1** CV experiments. Also, the large fwhm of the three carboranthiols analyzed, **M1** (140 ± 16 mV), **M9** (119 ± 28 mV), and **O1** (134 ± 24 mV), indicate less well packed structures than those for 1-dodecanethiol (74 ± 11 mV), which agrees with published STM images.[24,35]

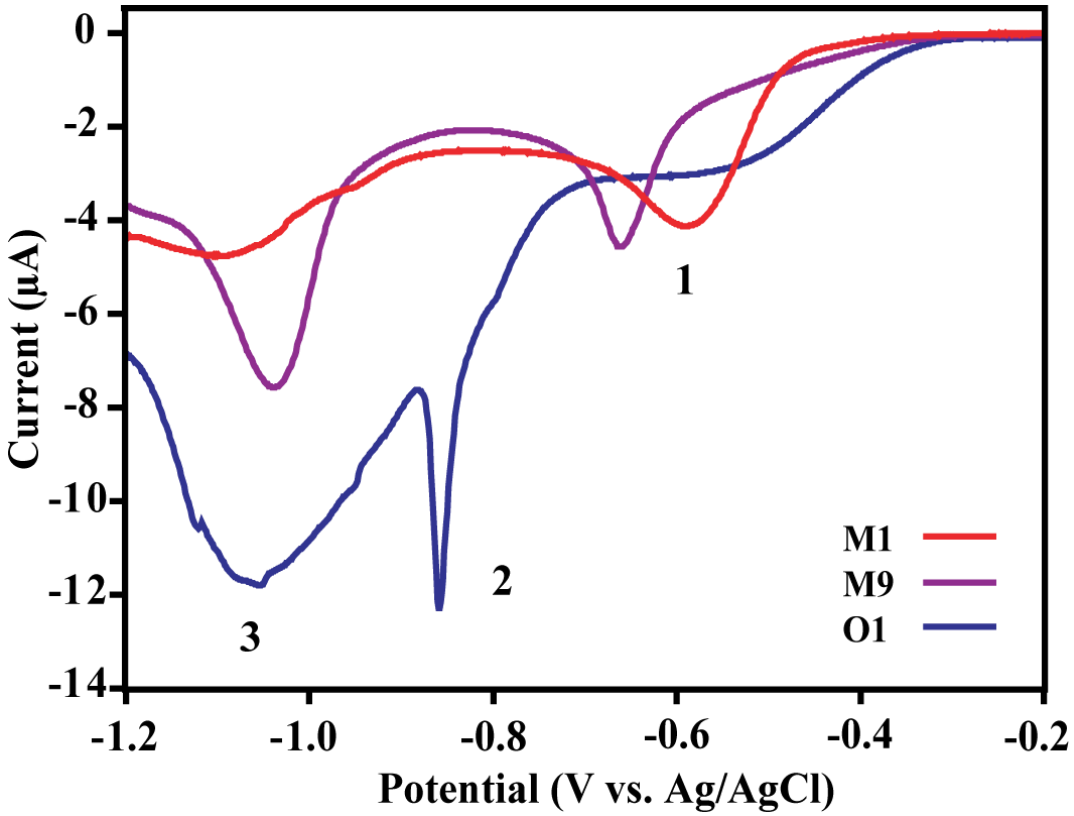

Figure 3.3: Individual cyclic voltammograms of **M1**, **M9**, and **O1** SAMs on Au{111} showing the first (1), second (2), and third (3) reductive current peaks.

Table 3.1: Collected values from cyclic voltammograms comparing the first reductive peak's properties, and **O1**'s peak 2.

		Average Peak Potential (mV)	Average Peak fwhm (mV)	Average Peak Current (μA)	Average Peak Area (μC)
Peak 1					
m-1-carboranethiolate	(**M1**)	-574 ± 26	127± 16	1.7 ± 0.6	9.7 ± 2.8
m-9-carboranethiolate	(**M9**)	-635 ± 75	114 ± 50	1.9 ± 0.9	8.3 ± 2.5
o-1-carboranethiolate	(**O1**)	-501 ± 26	134 ± 53	0.7 ± 0.1	5.2 ± 1.4
Peak 2					
o-1-carboranethiolate	(**O1**)	-860 ± 3	19.4 ± 2.5	5.5 ± 0.4	5.9 ± 1.2

Table 3.2: Collected values from cyclic voltammograms comparing the last reductive peak's properties.

		Average Peak Potential (mV)	Average Peak fwhm (mV)	Average Peak Current (μA)	Average Peak Area (μC)
Peak 3					
m-1-carboranethiolate	(**M1**)	-1079 ± 23	140 ± 16	1.5 ± 0.5	10.2 ± 4.2
m-9-carboranethiolate	(**M9**)	-1059 ± 23	119 ± 28	2.3 ± 1.6	12.4 ± 7.2
o-1-carboranethiolate	(**O1**)	-1056 ± 5	134 ± 24	1.7 ± 1.4	11.9 ± 10.9
n-dodecanethiolate	(**C12**)	-1098 ± 12	74 ± 11	5.3 ± 1.3	20.2 ± 4.9

From the data presented, it is evident that isomer-specific dipole-dipole interactions cause variations in molecular binding strengths. There are increased dipole-dipole interactions with neighboring molecules in **M1**, creating stronger binding energies. Isomers **M9** and **O1** have similar reductive potentials implying weaker dipole-dipole interactions between molecules, despite their large molecular dipole moments. Cyclic voltammetry of these molecules indicates several reductive reactions occur prior to thiol desorption at potentials higher than -1050 mV. All three isomers display the same weak, reductive peak at approximately -650 mV, which indicates the same electrochemical reaction that occurs in all carboranethiol molecules. Controlled potential electrolysis (discussed in Chapter 2) at -650 mV can be used with Fourier transform infrared spectroscopy (FTIR), x-ray photoelectric spectroscopy (XPS), and scanning tunneling microscopy (STM) to reveal possible changes in monolayer morphology. Cyclic voltammetry of non-thiolated carboranes can be useful in determining unbound carborane electrochemical behavior. There is a unique reductive reaction centered at -860 mV for **O1**; this is probably a result of carbon placement in the cage. Further electrochemical analysis of other *ortho*-carboranethiol isomers can be conducted to verify this, alongside further FTIR, XPS, and STM methods similar to those described previously. While results should differ between carboranethiols and **1ATC9**, employing similar methods to those discussed in Chapter 2 (e.g., CPE followed by STM imaging) may reveal insight into different reaction mechanisms. Further characterization of carboranethiolate SAMs can help in understanding how to control the self-assembly process, which can be beneficial for future nanoscale applications.

Chapter 4. Electrochemistry of *n*-Alkanethiols on Ge(111)

4.1 Germanium substrates for self-assembly

Semiconductors are important materials in solid-state devices because of their use in integrated circuits (ICs). Their properties can be easily manipulated by an applied electric field, incident light, or the addition of dopants; the addition of *n*-type or *p*-type dopants change the number and the type of majority charge carriers to electrons or holes, respectively.[47]

The group IV element Si is the dominant semiconductor for modern semiconductor devices. It is one of the most abundant elements on earth, has moderate electron and hole mobilities (1400 $\frac{cm^2}{Vs}$ and 450 $\frac{cm^2}{Vs}$, respectively), a relatively small band gap (1.12 eV), and an industrial infrastructure devoted to its manufacture.[47] The chemistry of silicon is also ideal for semiconductor devices. Silicon's native oxide, SiO_2, is an effective insulator and can be grown or chemically modified directly. Germanium is another group IV element that has attracted recent interest for high-speed semiconductor applications, especially for its high electron and hole mobilities (3900 $\frac{cm^2}{Vs}$ and 1900 $\frac{cm^2}{Vs}$, respectively) and small band gap (0.667 eV), which is half that of silicon.[47] Unfortunately, its native oxide layer is water-soluble, unstable, and is a poor insulator, resulting in charge "leaking" outside the bounds restricted by a device. Thiolated organic monolayers on germanium surfaces provide an opportunity to exert control over the interfacial chemistry of the germanium interface.[48-53] These thiol-modified surfaces using electrochemical techniques will be discussed in this chapter, which will offer to understand the characteristics of organic thiolates SAMs on semiconductor surface.

The working electrode acts as an electron collector and emitter in an electrochemical cell. The standard system requires the electrode to be conductive as well as electrochemically inert. A semiconductor can replace a metal electrode, but the problem lies in interfacing a semiconductor into the circuit. Typical semiconductor-metal interfaces follow the standard Schottky model.[47] The contact resistance is related to the electron barrier, or Schottky barrier height (SBH) (Φ_B), which in turn is related to the work function of the metal (Φ_M) and the electron affinity of the semiconductor (χ) by Equation 7.

$$\Phi_B = \Phi_M - \chi \qquad (7)$$

The SBH is the critical factor dictating the observed relationship between current (I) and voltage (V) in semiconductor junctions. A large SBH causes rectifying (or non-linear) behavior at the junction, while a small SBH will allow for an ohmic (or linear) I-V relationship. By measuring the I-V response of a junction, a linear response will thus represent an ohmic contact, while a nonlinear response signifies a Schottky junction. For electrochemical measurements, an ohmic contact on the working electrode is preferred.

Many semiconductor interfaces undergo Fermi-level pinning between the valence and the conduction band, resulting in a large SBH. In some cases, like Ge, the Fermi-level pinning is considered a result of metal-induced gap states (MIGS) that are created by permeating free electron wave functions from the metal.[54]

Ge undergoes a strong Fermi-level pinning close to the valence band.[55,56] This property makes it very easy to create a low SBH for *p*-type Ge, but very difficult for *n*-type Ge. The Schottky model can be applied to create a near-zero SB for *p*-type Ge by using a metal whose

work function is close to that of Ge. A relatively low SBH can be created on *n*-type Ge by reducing the influence of the free-electron wave function and by using a metal with a small work function. This can be accomplished by inserting an ultra-thin insulating film at the interface, for example GeO_x.[57,58] Here, contact resistance is a function of oxide thickness, as shown in Figure 4.1. If too thin, the metal's free electron wave function penetrates into the semiconductor. However, if it is too thick, the electron's tunneling resistance increases.

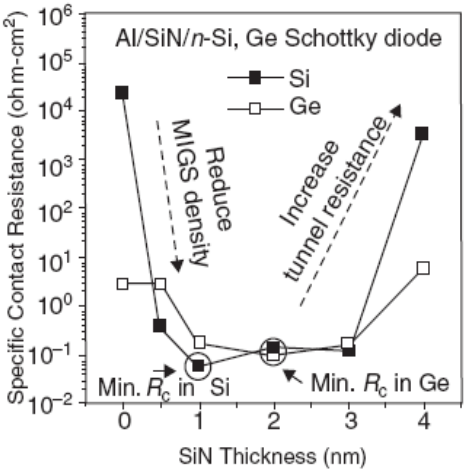

Figure 4.1. Diagram shows the relationship between contact resistance and ultra-thin oxide layer thickness. Here SiN is used as the insulating layer between germanium and an aluminum contact. This diagram is in agreement with the metal-induced gap states (MIGS) theory, which results in Fermi level pinning. Reproduced with permission from reference 59.

We determine the SBH by first finding the saturation current (I_s), which is determined by plotting the natural log of I against positive V. From the linear portion of this plot, the y-intercept yields I_s.[47] From this value, we can estimate the Φ_B from the following equation:

$$\Phi_B = \left(\frac{K_B T}{q}\right) \ln\left(\frac{AA^* T^2}{I_s}\right) \quad (8)$$

where, K_B is the Boltzmann's constant, T is temperature, q is the elementary charge, A is the area of the semiconductor, A^* is the Richardson's constant ($140 \frac{A}{cm^2 K^2}$ for *n*-type Ge).[59] Next, we investigate the ideality of the device by determining the ideality factor *n* using the following equation:

$$\ln(I) = \ln(I_s) + \left(\frac{q}{nK_B T}\right) V \quad (9)$$

The slope of the linear portion of the ln(I) vs. V plot can be used to determine *n*. An ideality factor greater than 1 is an indication of recombination and resistive losses.

4.2 Germanium Electrode Characterization

4.2.1 Procedure

Current-voltage characteristics are measured using an NI ENET-9219 data acquisition device from National Instruments (Austin, Texas) and analyzed using National Instruments' Labview 2009 SignalExpress. A model 81150A 120 MHz Pulse Function Arbitrary Generator from Agilent Technologies, Inc. (Santa Clara, California) is used to generate the current. Measurements are taken inside a 'black box' to ensure minimal light interference. Single-side-polished *n*-type germanium (111) (As-doped) wafers, (3 inch diameter, 375 µm thick, and resistivity between 0.005 – 0.002 $\frac{\Omega}{\text{cm}}$) are purchased from Silicon Quest International, Inc. (Santa Clara, California), and indium, for ohmic contacts is purchased from Sigma-Aldrich Co. (St. Louis, Missouri)

Au ($\Phi_M \approx 5.1$ eV)[60] and In ($\Phi_M \approx 4.09$ eV)[61] contacts are used for taking I-V measurements; the Au is in contact with the Ge(111) ($\Phi_S \approx 4.8$ eV)[62] interface, while indium is soldered on at 275 °C in two opposite locations on the same surface. Seven samples are used to determine the average value of the Schottky barrier heights.

4.2.2 Germanium I-V Characteristics

Figure 4.2 shows the current-voltage relationship of *n*-type germanium with an oxide passivation layer in contact with Au. It shows minimal current response at reverse bias, which is in the region of interest for electrochemical studies for thiol-modified electrodes and a turn-on voltage of approximately 200 mV. Therefore, it is necessary to have ohmic characteristics for voltages below this turn-on voltage. By adding indium contacts to the GeO_x-Ge interface, an ohmic junction can be formed (Figure 4.3). A SBH of 0.61 ± 0.01 eV with an ideality factor of 70.43 ± 5.05 was estimated using Equations 8 and 9, respectively. The SBH is substantially higher than desired, because using similar contacts can produce a SBH of 0.37 eV.[57] This larger SBH and very high ideality factor are most likely a result of improper contact formation, resulting in higher contact resistance.

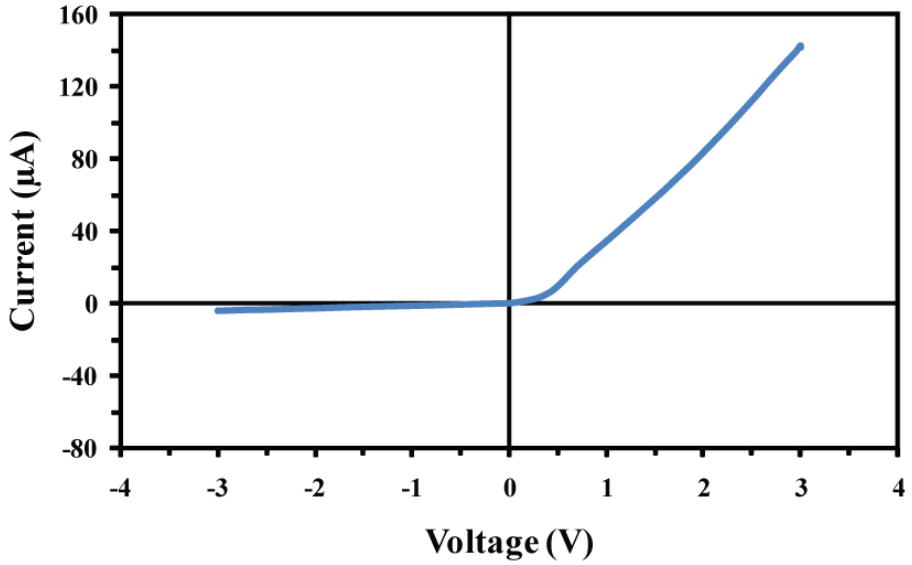

Figure 4.2. Current-voltage relationship of Au−GeO_x−Ge interface. Shows rectifying behavior with an approximate turn on voltage at 200 mV.

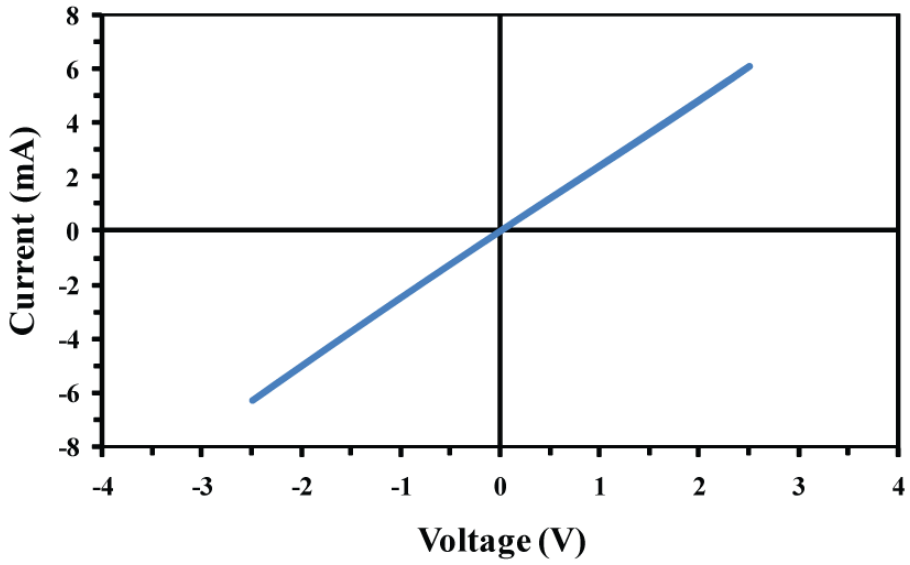

Figure 4.3. Current-voltage relationship of In−GeO_x−Ge interface, showing ohmic behavior, ideal for reverse bias applications.

4.3: Thiol-Modified Germanium Electrode

It is difficult to grow an insulating oxide similar to SiO_2 in Si devices. GeO_2 and GeO are not suitable for high-k gate oxides in metal-oxide semiconductor field effect transistors (MOSFETs). Removal of GeO_2/GeO alone cannot produce sufficient electrical properties. Surface passivation is required to keep GeO_x from reforming, and to act as an interfacial layer for another high-k dielectric. Thiolated SAMs on Ge can act as such a surface passivation layer. Cyclic voltammetry can be used to provide quantitative analysis about film uniformity and adsorbate-substrate and adsorbate-adsorbate interaction strengths.

A stronger reductive desorption potential is expected for thiolated SAMs on Ge(111) due to stronger Ge-S binding energy (~251 kJ/mol)[49] compared to the Au-S bond (~168 kJ/mol).[3] However, weaker adsorbate-adsorbate interactions have the opposite effect because of non-uniform Ge substrates; the molecular lattice with respect to the Ge surface has not been analytically determined, but other structural features have been determined.[48-50] Cyclic voltammetry may give insight on the molecular order, the extent of intermolecular interactions, and packing density. Figure 4.4 shows an example of a thiol-modified Ge(111)-In electrode.

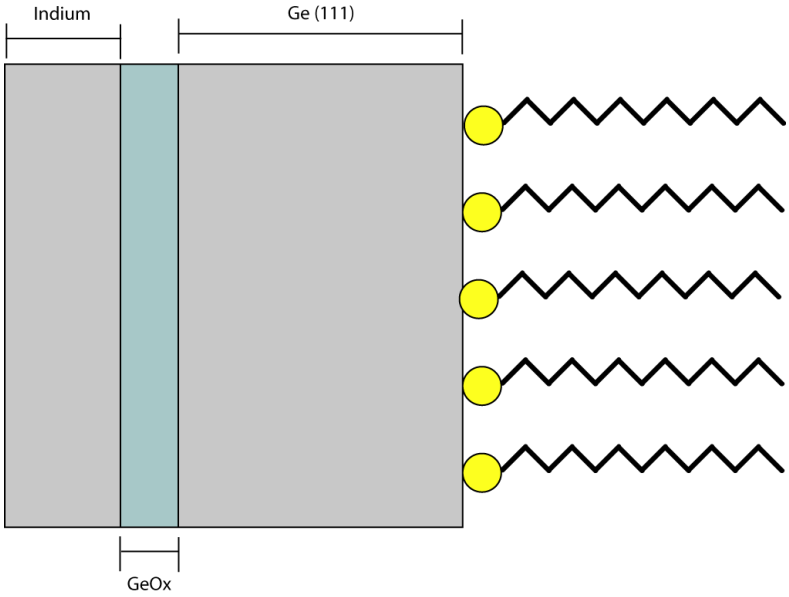

Figure 4.4. Proposed structure of thiol-modified germanium electrodes, suitable for electrochemical analysis. Indium is in contact with the ultra-thin oxide layer next to *n*-type Ge(111).

4.3.1 Self-Assembly of Organic Thiols on Ge (111)

Ge(111) substrates are prepared by soldering an In contact to the unpolished side. Samples of *n*-dodecanethiolate SAMs are prepared by immersing the Ge(111) substrate in a 0.5 mM solution of **C12** in a 1:1 ratio of deionized water and ethanol. Clean substrates are placed in solution at room temperature for 24 h. Following deposition, each sample is cleaned in the same way as described earlier. The samples are used immediately for electrochemical measurements.[63]

Using the equipment described in Section 1.2, an electrochemical cell potential is applied with a Ag/AgCl saturated KCl reference electrode and a Pt wire counter electrode. The supporting electrolyte, an aqueous solution of 20 mM H_2SO_4 (95-98% A.C.S. [grade], Sigma-Aldrich, St Louis, MO), is prepared with deionized water (18.2 M, Millipore Corp. Billerica, MA) and purged with ultrahigh purity N_2 for 30 min. Cyclic voltammetry is performed at reductive potentials of +200 to -2500 mV with a scan rate of 40 mV/s. Baseline correction of voltammograms are done using the previously described method in Section 2.3.1. Eight representative cyclic voltammograms are selected to calculate the peak positions, peak areas, and peak fwhm's with their respective standard deviations for **C12** on *n*-type Ge (111).

4.3.2 Voltammetric Desorption of Thiolated Ge

Cyclic voltammograms of **C12**-modified Ge(111) electrodes show a reductive potential peak centered at -2044 ± 175 mV, much higher than for thiol desorption potentials on Au{111} substrates (Figure 4.5). This higher reductive potential is primarily a result of increased substrate-adsorbate interactions. A large fwhm may indicate poor molecular ordering. The large peak current (89 ± 16 μA), nearly 18 times larger than that of Au{111}) and a large standard deviation makes it difficult to have substantial conclusions.

The large peak current can be attributed to current generation from solvent breakdown, which normally occurs on Ge at -880 mV. This effect does not occur before thiol reduction because the SAM acts as a potential barrier. The insulating monolayer prevents solvent–Ge interactions. Due to a poorly ordered SAM structure, supported by a large fwhm (198 ± 52 mV), **C12** thiols do not necessarily desorb together because of the lack of stabilizing intermolecular interactions. When a thiol is removed from the substrate it opens new reaction sites where water hydrolysis can occur, a process that accelerates as more thiolates desorb. This effect gives rise to a large increase in current. The substantially large standard deviation implies substantial inconsistencies in reductive desorption. Further, inconsistencies in the soldering of the In contacts induces further variability in these measurements.

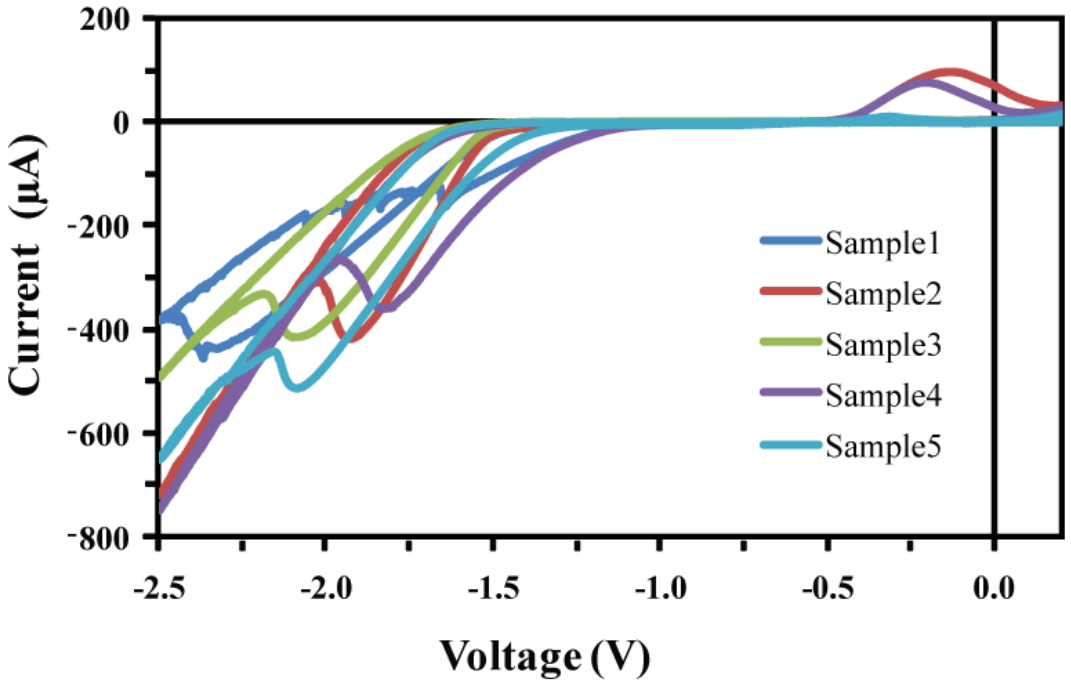

Figure 4.5. Reductive desorption of *n*-dodecanethiolate from Ge(111) in 20mM H_2SO_4 at room temperature. The cause for the oxidative peaks is unknown.

Table 4.1: Collected values from cyclic voltammograms comparing the reductive peak properties of *n*-dodecanethiolate on Ge(111) and Au{111}

	Average Peak Potential (mV)	Average Peak fwhm (mV)	Average Peak Current (μA)	Average Peak Area (µC)
n-dodecanethiolate (**C12**) on Ge(111)	-2044 ± 175	198 ± 52	89 ± 16	416 ± 125
n-dodecanethiolate (**C12**) on Au{111}	-1098 ± 12	74 ± 11	5.3 ± 1.3	20.2 ± 4.9

Results show that thiolate SAMs alter the Ge surface chemistry. The high reductive desorption potential is consistent with the high bond energy of S-Ge relative S-Au. However, many variables remain to be addressed before we can make concrete claims about the correlations between cyclic voltammetric analysis of SAMs supported on Au and Ge. The wide range of reductive peak potentials observed for SAMs on Ge means several experimental changes need to be made. Critical variables include contact formation, SAM deposition, and solvent environment. Consistent, reliable contacts can be formed on *p*-type Ge by chemical vapor deposition, which will help eliminate variability from differences in contact resistance. Second, changes in sample to sample SAM quality remain a challenge; a next step would be deposition at a higher temperature to improve overall SAM quality and consistency. Other methods for SAM deposition on Ge can be used and compared to our preparation method, with a focus on strategies to limit surface roughness. Finally, choosing a solvent with a breakdown voltage larger than the thiol desorption potential can eliminate the observed excess current. Refining the experiment and interpreting the results will firmly establish electrochemical analyses as a principal method for the analysis of semiconducting germanium interfaces.

Chapter 5: Conclusions and Future Prospects

Electrochemistry on self-assembled monolayers of amide-containing alkanethiols and cage thiols on Au{111} allows us to evaluate the role of hydrogen-bonding interactions and dipole-dipole interactions within a monolayer. The buried amide functional group incorporated into the alkyl backbone strongly influences molecular interactions within the monolayer, with interactions dominated by hydrogen-bonding. In general, relatively large cage thiols have lower van der Waals interactions, but carboranethiols introduce strong dipole-dipole interactions in different dipole orientations depending on the positions of carbon and boron atoms in the cage. Also, electrochemical characterization of alkanethiolate (**C12**) monolayers on Ge(111) shows the effect of stronger adsorbate-substrate interactions.

Networked hydrogen-bonds within **1ATC9** monolayers give larger reductive potentials than *n*-alkanethiolate SAMs. When more thermal energy was provided during assembly (by elevating solution temperature) individual molecules align into the most favorable orientations, *linear* hydrogen bonding networks, maximizing intermolecular interactions. The presence of a double peak in **1ATC9** cyclic voltammograms was further investigated using controlled potential electrolysis and STM imaging. Applying potentials slightly more negative than the first reduction causes monolayer reorganization, resulting in the formation of an unusual nanostructure. Detailed studies on amide-containing alkanethiolate monolayers with various number and position of amides should be considered in order to extend our understanding of the hydrogen-bonding networks within monolayers.

The higher reductive potential of **M1** compared to both the **M9** and **O1** isomers is due to the stronger and more favorable dipole-dipole interactions. The dipole moment of **M1** is positioned parallel to the substrate, while the dipole moment of **M9** is oriented vertically, with the positive end away from the substrate. Based on the calculated result of **M1** and **M9**, we predict that the dipole moment of **O1** is oriented nearly normal, with the positive pole close to the substrate. The presence of a sharp peak at -860 mV in the **O1** voltammograms can be explained by this dipole orientation. When the reductive potential increases, higher negative charge builds up on the Au electrode, resulting in an increasingly favorable dipole arrangement in **O1** until monolayer desorption, unlike **M1** or **M9**.

The high desorption potential for **C12** on a Ge(111) substrate is a result of the strong substrate-adsorbate bond, which is higher than that for the gold-sulfur bond. Quantitative analysis was difficult due to the large current generation and variability between reductive potentials. Future research needs to be conducted to minimize both the extra current generation and to improve consistency in Ge SAM reductive potentials.

Electrochemistry on organic thiolate monolayer systems on Au and Ge substrates provides insight into the interactions beyond van der Waals forces, specifically the hydrogen-bonding and dipole-dipole, and adsorbate-substrate interactions that control the structure and properties of SAMs. My studies on these factors on organic-metal interfaces will help in the development of a strategy on how to tune these interactions to gain better control over tailored molecular nanostructures.

REFERENCES

(1) Brown, T. L.; LeMay, H. E.; Bursten, B. E.; Murphy, C. J. *Chemistry: A Central Science*; 11 ed.; Pearson Education, Inc.: Upper Saddle River, 2009.

(2) Bard, A. J.; Faulkner, L. R. *Electrochemical Methods: Fundamentals and Applications*; John Wiley and Sons, Inc: Hoboken, 2001.

(3) Love, J. C.; Estroff, L. A.; Kriebel, J. K.; Nuzzo, R. G.; Whitesides, G. M. *Chemical Reviews* **2005**, *105*, 1103-1169.

(4) Smith, R. K.; Lewis, P. A.; Weiss, P. S. *Progress in Surface Science* **2004**, *75*, 1-68.

(5) Schwartz, D. K. *Annual Review of Physical Chemistry* **2001**, *52*, 107-137.

(6) Chailapakul, O.; Sun, L.; Xu, C. J.; Crooks, R. M. *Journal of the American Chemical Society* **1993**, *115*, 12459-12467.

(7) Kim, K. S.; Kang, M. S.; Ma, H.; Jen, A. K. Y. *Chemistry of Materials* **2004**, *16*, 5058-5062.

(8) Haussling, L.; Knoll, W.; Ringsdorf, H.; Schmitt, F. J.; Yang, J. L. *Makromolekulare Chemie-Macromolecular Symposia* **1991**, *46*, 145-155.

(9) Kuhn, H.; Ulman, A. *Thin Films*; Academic Press: New York, 1995; Vol. 20.

(10) Zhong, C. J.; Porter, M. D. *Journal of Electroanalytical Chemistry* **1997**, *425*, 147-153.

(11) Kakiuchi, T.; Usui, H.; Hobara, D.; Yamamoto, M. *Langmuir* **2002**, *18*, 5231-5238.

(12) Sumi, T.; Wano, H.; Uosaki, K. *Journal of Electroanalytical Chemistry* **2003**, *550*, 321-325.

(13) Wong, S. S.; Porter, M. D. *Journal of Electroanalytical Chemistry* **2000**, *485*, 135-143.

(14) Zhong, C. J.; Zak, J.; Porter, M. D. *Journal of Electroanalytical Chemistry* **1997**, *421*, 9-13.

(15) Dubois, L. H.; Zegarski, B. R.; Nuzzo, R. G. *Journal of Chemical Physics* **1993**, *98*, 678-688.

(16) Schreiber, F. *Progress in Surface Science* **2000**, *65*, 151-256.

(17) Dubois, L. H.; Nuzzo, R. G. *Annual Review of Physical Chemistry* **1992**, *43*, 437-463.

(18) Dameron, A. A.; Mullen, T. J.; Hengstebeck, R. W.; Saavedra, H. M.; Weiss, P. S. *Journal of Physical Chemistry C* **2007**, *111*, 6747-6752.

(19) Mullen, T. J.; Dameron, A. A.; Andrews, A. M.; Weiss, P. S. *Aldrichimica Acta* **2007**, *40*, 21-31.

(20) Mullen, T. J.; Dameron, A. A.; Saavedra, H. M.; Williams, M. E.; Weiss, P. S. *Journal of Physical Chemistry C* **2007**, *111*, 6740-6746.

(21) Saavedra, H. M.; Barbu, C. M.; Dameron, A. A.; Mullen, T. J.; Crespi, V. H.; Weiss, P. S. *Journal of the American Chemical Society* **2007**, *129*, 10741-10746.

(22) Hohman, J. N.; Claridge, S. A.; Kim, M.; Weiss, P. S. *Elsevier* **2010**, *70*, 188-208.

(23) Base, T.; Bastl, Z.; Plzak, Z.; Grygar, T.; Plesek, J.; Carr, M. J.; Malina, V.; Subrt, J.; Bohacek, J.; Vecernikova, E.; Kriz, O. *Langmuir* **2005**, *21*, 7776-7785.

(24) Hohman, J. N.; Zhang, P. P.; Morin, E. I.; Han, P.; Kim, M.; Kurland, A. R.; McClanahan, P. D.; Balema, V. P.; Weiss, P. S. *ACS Nano* **2009**, *3*, 527-536.

(25) Balss, K. M.; Coleman, B. D.; Lansford, C. H.; Haasch, R. T.; Bohn, P. W. *Journal of Physical Chemistry B* **2001**, *105*, 8970-8978.

(26) Imabayashi, S.; Iida, M.; Hobara, D.; Feng, Z. Q.; Niki, K.; Kakiuchi, T. *Journal of Electroanalytical Chemistry* **1997**, *428*, 33-38.

(27) Walczak, M. M.; Popenoe, D. D.; Deinhammer, R. S.; Lamp, B. D.; Chung, C. K.; Porter, M. D. *Langmuir* **1991**, *7*, 2687-2693.

(28) Widrig, C. A.; Chung, C.; Porter, M. D. *Journal of Electroanalytical Chemistry* **1991**, *310*, 335-359.

(29) Sabatani, E.; Rubinstein, I.; Maoz, R.; Sagiv, J. *Journal of Electroanalytical Chemistry* **1987**, *219*, 365-371.

(30) Sabatani, E.; Rubinstein, I. *Journal of Physical Chemistry* **1987**, *91*, 6663-6669.

(31) Sabatani, E.; Cohenboulakia, J.; Bruening, M.; Rubinstein, I. *Langmuir* **1993**, *9*, 2974-2981.

(32) Yang, D. F.; Wilde, C. P.; Morin, M. *Langmuir* **1996**, *12*, 6570-6577.

(33) Yang, D. F.; Wilde, C. P.; Morin, M. *Langmuir* **1997**, *13*, 243-249.

(34) Byloos, M.; Al-Maznai, H.; Morin, M. *Journal of Physical Chemistry B* **1999**, *103*, 6554-6561.

(35) Mullen, T. J.; Dameron, A. A.; Weiss, P. S. *Journal of Physical Chemistry B* **2006**, *110*, 14410-14417.

(36) Clegg, R. S.; Hutchison, J. E. *Langmuir* **1996**, *12*, 5239-5243.

(37) Clegg, R. S.; Hutchison, J. E. *Journal of the American Chemical Society* **1999**, *121*, 5319-5327.

(38) Clegg, R. S.; Reed, S. M.; Hutchison, J. E. *Journal of the American Chemical Society* **1998**, *120*, 2486-2487.

(39) Lewis, P. A.; Smith, R. K.; Kelly, K. F.; Bumm, L. A.; Reed, S. M.; Clegg, R. S.; Gunderson, J. D.; Hutchison, J. E.; Weiss, P. S. *Journal of Physical Chemistry B* **2001**, *105*, 10630-10636.

(40) Smith, R. K.; Reed, S. M.; Lewis, P. A.; Monnell, J. D.; Clegg, R. S.; Kelly, K. F.; Bumm, L. A.; Hutchison, J. E.; Weiss, P. S. *Journal of Physical Chemistry B* **2001**, *105*, 1119-1122.

(41) Besocke, K. *Surface Science* **1987**, *181*, 145-153.

(42) Frohn, J.; Wolf, J. F.; Besocke, K.; Teske, M. *Review of Scientific Instruments* **1989**, *60*, 1200-1201.

(43) Tamchang, S. W.; Biebuyck, H. A.; Whitesides, G. M.; Jeon, N.; Nuzzo, R. G. *Langmuir* **1995**, *11*, 4371-4382.

(44) Kim, M.; Hohman, J. N.; Serino, A. C. *Journal of Physical Chemistry* **2010**, *114*, 19744-19751.

(45) Kim, M.; Hohman, J. N.; Morin, E. I.; Daniel, T. A.; Weiss, P. S. *Journal of Physical Chemistry A* **2009**, *113*, 3895-3903.

(46) Hohman, J. N.; Kim, M.; Houk, J. K.; Weiss, P. S. 2010.

(47) Kasap, S. O. *Principles of Electronic Materials and Devices*; 3 ed.; McGraw-Hill: New York, 2006; Vol. 1.

(48) Kachian, J. S.; Wong, K. T.; Bent, S. F. *Accounts of Chemical Research* **2010**, *43*, 346-355.

(49) Ardalan, P.; Musgrave, C. B.; Bent, S. F. *Langmuir* **2009**, *25*, 2013-2025.

(50) Ardalan, P.; Sun, Y.; Pianetta, P.; Musgrave, C. B.; Bent, S. F. *Langmuir* **2010**, *26*, 8419-8429.

(51) Holmberg, V. C.; Korgel, B. A. *Chemistry of Materials* **2010**, *22*, 3698-3703.

(52) Knapp, D.; Brunschwig, B. S.; Lewis, N. S. *Journal of Physical Chemistry C* **2010**, *114*, 12300-12307.

(53) Gregory, B. W.; Thomas, S.; Stephens, S. M.; Dluhy, R. A.; Bottomley, L. A. *Langmuir* **1997**, *13*, 6146-6150.

(54) Dimoulas, A.; Toriumi, A.; Mohney, S. E. *MRS Bulletin* **2009**, *34*, 522-529.

(55) Dimoulas, A.; Tsipas, P.; Sotiropoulos, A.; Evangelou, E. K. *Applied Physics Letters* **2006**, *89*, 1-3.

(56) Nishimura, T.; Kita, K.; Toriumi, A. *Applied Physics Letters* **2007**, *91*, 1-3.

(57) Nishimura, T.; Kita, K.; Toriumi, A. *Applied Physics Express* **2008**, *1*, 1-3.

(58) Lieten, R. R.; Degroote, S.; Kuijk, M.; Borghs, G. *Applied Physics Letters* **2008**, *92*, 1-3.

(59) Sze, S. M. *Physics of Semiconductor Interfaces*; Wiley: New York, 1981.

(60) Tripler, P. A.; Llewellyn, R. A. *Modern Physics*; 4 ed.; W. H. Freeman and Company: New York, 1999.

(61) *Handbook of Chemistry and Physics*; 91 ed.; Taylor and Francis Group, LLC, 2010.

(62) Gobeli, G. W.; Allen, F. G. *Surface Science* **1964**, *2*, 402-408.

(63) Hohman, J. N.; Kim, M.; Lawrence, J. A.; McClanahan, P. D.; Weiss, P. S. 2010, 1-22.